SpezialForschungsBereich F 32

Karl–Franzens Universität Graz
Technische Universität Graz
Medizinische Universität Graz

Application of the reciprocity principle for the determination of planar cracks in piezoelectric material

P. Steinhorst B. Kaltenbacher

SFB-Report No. 2011-025 October 2011

A–8010 GRAZ, HEINRICHSTRASSE 36, AUSTRIA

Supported by the
Austrian Science Fund (FWF)

SFB sponsors:

- **Austrian Science Fund** (FWF)
- **University of Graz**
- **Graz University of Technology**
- **Medical University of Graz**
- **Government of Styria**
- **City of Graz**

Application of the reciprocity principle for the determination of planar cracks in piezoelectric material

Peter Steinhorst*, Barbara Kaltenbacher*

Abstract

Piezoelectricity is a coupling between the electrical and the mechanical behaviour of certain materials, which is exploited in a wide range of transducer applications. By far most of the piezoelectric devices nowadays consist of ceramics, which are known as brittle material. Therefore, the detection of cracks in piezoelectric ceramics from external measurements in the sense of nondestructive testing is a task which is of high practical interest.

This paper is a further extension of a method using the reciprocity principle, which has been introduced by Andrieux, Ben Abda et. al in the context of linear [2] isotropic electrostatics, and in the case of isotropic linear elasticity [1]. As preliminary work we use a first extension of the method concerning crack plane determination in anisotropic linear elasticity [14], especially including the case of transversal isotropy like in the elastic part of the piezoelectric material tensor. Our extension of [2] and [14] provides a method which is applicable for crack plane determination in piezoelectrics, using only data from the outer boundary.

Also a 2D-implementation in an existing FEM-software has been carried out to test the method on some numerical examples.

Contents

*Institut für Mathematik, Alpen-Adria-Universität Klagenfurt, Universitätsstraße 65-67, A-9020 Klagenfurt. Email: peter.steinhorst@aau.at, barbara.kaltenbacher@aau.at

1 Mathematical formulation

1.1 The forward problem

Let Ω be a bounded Lipschitz domain in $\mathbb{R}^d$ ($d \in \{2,3\}$), and the crack Σ a surface in $\Omega \subset \mathbb{R}^3$ or a curve in $\Omega \subset \mathbb{R}^2$ with sufficient smoothness. Σ need not necessarily be simply connected, it may also consist of several pieces. We restrict ourselves to planar cracks, i.e., $\Sigma \subset \Pi$ where Π is a plane in $\mathbb{R}^3$ or a line in $\mathbb{R}^2$. The whole boundary Γ of the cracked domain $\Omega \setminus \Sigma$ consists of the outer boundary $\partial\Omega$ and the crack faces of Σ.
The primary fields will be denoted by

- $u : \Omega \to \mathbb{R}^d$ the displacement field,
- $\varphi : \Omega \to \mathbb{R}$ the scalar electric potential field.

The strain tensor ε denotes the symmetric part of the displacement gradient:

$$\varepsilon(u) = (\nabla u)^s := \frac{1}{2}\left(\nabla u + (\nabla u)^\top\right), \quad \text{i.e.} \quad \varepsilon_{ij}(u) = \frac{1}{2}\left(\frac{\partial u_i}{\partial u_j} + \frac{\partial u_j}{\partial u_i}\right). \tag{1}$$

The stress tensor σ and the dielectric displacement D are coupled via the linear piezoelectric material law:

$$\begin{array}{rcccl} \sigma(u,\varphi) & = & C : \varepsilon(u) & + & B \cdot \nabla\varphi \quad , \\ D(u,\varphi) & = & B^\top : \varepsilon(u) & - & K \cdot \nabla\varphi \quad , \end{array} \tag{2}$$

The material tensors are

- $C = C_{ijkl}$ – the elastic material tensor (of 4th order)
- $K = \kappa_{ij}$ – the dielectric tensor (of 2nd order)
- $B = \mathbf{e}_{ijk}$ – the piezoelectric coupling tensor (of 3rd order)

Inside $\Omega \setminus \Sigma$ we postulate the absence of volume forces and charges, which corresponds to the source free static piezoelectric differential equations:

$$\begin{array}{rcl} \operatorname{div} \sigma(u,\varphi) & = & \mathbf{0}\,, \\ \operatorname{div} D(u,\varphi) & = & 0\,. \end{array} \tag{3}$$

The boundary conditions are choosen of Neumann type in both fields, with given mechanical forces and electric charges on the outer boundary:

$$\sigma(u,\varphi)\mathfrak{n} = F\,, \quad D(u,\varphi)\cdot\mathfrak{n} = g \qquad \text{on } \partial\Omega\,. \tag{4}$$

Denote the crack faces by Σ^+ and Σ^-. We introduce the following notation for the jumps of u and φ over Σ:

$$[\![u]\!] = u|_{\Sigma^+} - u|_{\Sigma^-}\,, \quad [\![\varphi]\!] = \varphi|_{\Sigma^+} - \varphi|_{\Sigma^-}\,.$$

One of the following boundary conditions is supposed to hold on the crack:

- traction free and impermeable conditions, which is the simplest case

$$\sigma(u,\varphi)N = \mathbf{0}\,, \quad D(u,\varphi)\cdot N = 0 \qquad \text{on } \Sigma\,. \tag{5}$$

- traction free and semipermeable conditions

$$\sigma(u,\varphi)N = \mathbf{0}\,, \quad D^+(u,\varphi)\cdot N = D^-(u,\varphi)\cdot N = -\kappa_{\mathrm{L}}\frac{[\![\varphi]\!]}{[\![u]\!]\cdot N} \qquad \text{on } \Sigma\,. \tag{6}$$

Here, $\mathfrak{n}$ denotes the outer normal of $\partial\Omega$ and N the normal of the crack plane Π, which is unique up to orientation and without loss of generality can be assumed to be the outer normal of the crack face Σ^+. Both $\mathfrak{n}$ and N are normalized to $\|\mathfrak{n}\| = \|N\| = 1$.

Remark: *The assumption of traction-free and charge-free crack faces is often not a very realistic model in piezoelectricity, even in the absence of crack closing. Because of the expected small crack opening, the electric potentials on both sides of the crack influence each other. If a potential difference exists, a strong electric field inside the crack may result. This leads to other more realistic models like semipermeable boundary conditions (6), see [4], which are more complicated than the charge-free ones, though. A second effect which might influence the field distribution significantly, is the electrostatic attraction of the crack faces. This can also be considered in a modification of the elastic boundary conditions as compared to the simple traction-free assumption [8],[5].*
The case of crack closing and contact between crack faces adds further challenges to the mathematical model and the numerical solution of crack simulation, cf., e.g., [10].

An equivalent matrix-vector-notation of (2) using VOIGTs index mapping is written as

$$\begin{pmatrix} \underline{\sigma}(u,\varphi) \\ D(u,\varphi) \end{pmatrix} = \begin{pmatrix} \underline{\underline{C}} & \underline{\underline{B}} \\ \underline{\underline{B}}^\top & -\underline{\underline{K}} \end{pmatrix} \begin{pmatrix} \underline{\varepsilon}(u) \\ \nabla\varphi \end{pmatrix} =: A \begin{pmatrix} \underline{\varepsilon}(u) \\ \nabla\varphi \end{pmatrix} . \tag{7}$$

Here, the material matrices in the 3D transversally isotropic case have the following structure:

$$\underline{\underline{C}} = \begin{pmatrix} c_{11} & c_{12} & c_{13} & 0 & 0 & 0 \\ c_{12} & c_{11} & c_{13} & 0 & 0 & 0 \\ c_{13} & c_{13} & c_{33} & 0 & 0 & 0 \\ 0 & 0 & 0 & c_{44} & 0 & 0 \\ 0 & 0 & 0 & 0 & c_{44} & 0 \\ 0 & 0 & 0 & 0 & 0 & c_{66} \end{pmatrix}, \quad \underline{\underline{B}} = \begin{pmatrix} 0 & 0 & e_{13} \\ 0 & 0 & e_{13} \\ 0 & 0 & e_{33} \\ 0 & e_{61} & 0 \\ e_{61} & 0 & 0 \\ 0 & 0 & 0 \end{pmatrix}, \quad \underline{\underline{K}} = \begin{pmatrix} \kappa_{11} & 0 & 0 \\ 0 & \kappa_{11} & 0 \\ 0 & 0 & \kappa_{33} \end{pmatrix},$$

with x_3 as poling direction and $c_{66} = \frac{1}{2}(c_{11} - c_{12})$. Here the stress and strain components are written in vectors

$$\underline{\sigma} = (\sigma_{11}, \sigma_{22}, \sigma_{33}, \sigma_{23}, \sigma_{13}, \sigma_{12})^\top , \qquad \underline{\varepsilon} = (\varepsilon_{11}, \varepsilon_{22}, \varepsilon_{33}, 2\varepsilon_{23}, 2\varepsilon_{13}, 2\varepsilon_{12})^\top \quad \text{in 3D} .$$

In the 2D case as electromechanical extension of the plain strain mode we have:

$$\underline{\underline{C}} = \begin{pmatrix} c_{11} & c_{12} & 0 \\ c_{12} & c_{22} & 0 \\ 0 & 0 & c_{33} \end{pmatrix}, \ \underline{\underline{B}} = \begin{pmatrix} 0 & e_{12} \\ 0 & e_{22} \\ e_{31} & 0 \end{pmatrix}, \ \underline{\underline{K}} = \begin{pmatrix} \kappa_{11} & 0 \\ 0 & \kappa_{22} \end{pmatrix},$$

$$\text{and} \qquad \underline{\sigma} = (\sigma_{11}, \sigma_{22}, \sigma_{12})^\top , \qquad \underline{\varepsilon} = (\varepsilon_{11}, \varepsilon_{22}, 2\varepsilon_{12})^\top .$$

Note that now x_2 denotes the poling direction, due to this fact the 2D indexing of the elastic components has been changed in comparison to the 3D notation and also to the notation used in [14].

As noted in [1] and shortly explained in [14], additional constraints are necessary to ensure existence and uniqueness of a solution in the case of pure NEUMANN problems.
Extending these considerations to a piezoelectric material without inner sources (3) in the uncracked domain Ω, the following conditions on the (outer) boundary have to be fulfilled within (4) to ensure the existence of a solution of (3),(4):

$$\int_{\partial\Omega} F \, dS = \mathbf{0} , \qquad \int_{\partial\Omega} x \times F \, dS = \mathbf{0} , \qquad \int_{\partial\Omega} g \, dS = 0 . \tag{8}$$

Violation of these conditions would prevent the body from achieving a static equilibrium in a kinematic and electric sense.

To ensure uniqueness, the primary fields of the solution also have to be restricted by some conditions

$$\int_{\partial\Omega} u\,dS = \mathbf{0}\,, \qquad \int_{\partial\Omega} x \times u\,dS = \mathbf{0}\,, \qquad \int_{\partial\Omega} \varphi\,dS = 0\,. \tag{9}$$

These conditions fix the body in space in the sense that they eliminate the degrees of freedom for kinematic rigid motions (translations, rotations) and the addition of a constant electric potential.

Derivation In order to justify equations (8) and (9), we denote in the 3D case

$$\mathbf{U} = \begin{pmatrix} u_1 \\ u_2 \\ u_3 \\ \varphi \end{pmatrix}, \ \mathbf{V} = \begin{pmatrix} v_1 \\ v_2 \\ v_3 \\ \psi \end{pmatrix}, \ \mathbf{F} = \begin{pmatrix} f_1 \\ f_2 \\ f_3 \\ g \end{pmatrix}, \quad \mathcal{B} = \left(\begin{array}{cccccc|c} \partial_{x_1} & 0 & 0 & 0 & \partial_{x_3} & \partial_{x_2} & \\ 0 & \partial_{x_2} & 0 & \partial_{x_3} & 0 & \partial_{x_1} & \\ 0 & 0 & \partial_{x_3} & \partial_{x_2} & \partial_{x_1} & 0 & \\ \hline & & & & & & \partial_{x_1} \quad \partial_{x_2} \quad \partial_{x_3} \end{array}\right)^\top,$$

furthermore

$$\mathcal{N} = \left(\begin{array}{cccccc|c} n_1 & 0 & 0 & 0 & n_3 & n_2 & \\ 0 & n_2 & 0 & n_3 & 0 & n_1 & \\ 0 & 0 & n_3 & n_2 & n_1 & 0 & \\ \hline & & & & & & n_1 \quad n_2 \quad n_3 \end{array}\right)^\top \quad \text{where } \mathfrak{n} = \begin{pmatrix} n_1 \\ n_2 \\ n_3 \end{pmatrix} \text{ the outer normal of } \Omega\,.$$

The generalized Green's formula for linear piezoelectricity reads

$$-\int_\Omega \mathcal{B}^\top A\mathcal{B}\mathbf{U} \cdot \mathbf{V}\,dx = \int_\Omega A\mathcal{B}\mathbf{U} \cdot \mathcal{B}\mathbf{V}\,dx - \int_{\partial\Omega} \mathcal{N}^\top A\mathcal{B}\mathbf{U} \cdot \mathbf{V}\,dS\,.$$

We have $\mathcal{B}\mathbf{U} = \mathbf{0}$ if and only if $\varepsilon(u) = \mathbf{0}$ and $\nabla\varphi = \mathbf{0}$. The space $\mathcal{R}$ of rigid motions has dimension 7 with basis vectors

$$\begin{pmatrix} 1 \\ 0 \\ 0 \\ 0 \end{pmatrix}, \begin{pmatrix} 0 \\ 1 \\ 0 \\ 0 \end{pmatrix}, \begin{pmatrix} 0 \\ 0 \\ 1 \\ 0 \end{pmatrix}, \begin{pmatrix} 0 \\ 0 \\ 0 \\ 1 \end{pmatrix}, \begin{pmatrix} \begin{pmatrix} 1 \\ 0 \\ 0 \end{pmatrix} \times \begin{pmatrix} x_1 \\ x_2 \\ x_3 \end{pmatrix} \\ 0 \end{pmatrix}, \begin{pmatrix} \begin{pmatrix} 0 \\ 1 \\ 0 \end{pmatrix} \times \begin{pmatrix} x_1 \\ x_2 \\ x_3 \end{pmatrix} \\ 0 \end{pmatrix}, \begin{pmatrix} \begin{pmatrix} 0 \\ 0 \\ 1 \end{pmatrix} \times \begin{pmatrix} x_1 \\ x_2 \\ x_3 \end{pmatrix} \\ 0 \end{pmatrix}.$$

Thus, the solvability and uniqueness conditions read:

$$\int_{\partial\Omega} F_i\,dS = 0\,,\ i = 1,2,3,4\,; \quad \int_{\partial\Omega} x \times \begin{pmatrix} f_1 \\ f_2 \\ f_3 \end{pmatrix} dS = 0\,,$$

$$\int_{\partial\Omega} U_i\,dS = 0\,,\ i = 1,2,3,4\,; \quad \int_{\partial\Omega} x \times \begin{pmatrix} u_1 \\ u_2 \\ u_3 \end{pmatrix} dS = 0\,.$$

The proof is similar to the linear elastic case [14].

Variational formulation

Let $\mathbb{V}_0 \subset [H^1(\Omega\setminus\Sigma)]^{d+1}$ be the space of functions, which satisfy the conditions (9). Multiplication of the problem (3),(4),(5) with test functions v (displacement) and ψ (potential) and subsequent integration over $\Omega \setminus \Sigma$ leads to the following corresponding variational formulation:

$$\int_{\Omega\setminus\Sigma} [\sigma(u,\varphi) : \varepsilon(v) + D(u,\varphi)\cdot\nabla\psi]\,dx = \int_{\partial\Omega} [F\cdot v + g\psi]\,dS \qquad \forall (v,\psi) \in \mathbb{V}_0\,. \tag{10}$$

The variational formulation corresponding to the semipermeable crack problem (3),(4),(6) reads as

$$\begin{aligned}\int_{\Omega\setminus\Sigma} [\sigma(u,\varphi) : \varepsilon(v) + D(u,\varphi)\cdot\nabla\psi]\; dx &= \int_{\partial\Omega} [F\cdot v + g\psi]\; dS + \int_\Sigma (\psi^+ - \psi^-) D^+(u,\varphi)\cdot N\, dS \\ &= \int_{\partial\Omega} [F\cdot v + g\psi]\; dS - \kappa_{\mathrm{L}} \int_\Sigma \frac{[\![\varphi]\!][\![\psi]\!]}{[\![u]\!]\cdot N} dS \qquad \forall (v,\psi)\in \mathbb{V}_0\,. \end{aligned} \tag{11}$$

The occuring nonlinearity in the right hand side of problem (11) makes the (approximate) solution more tricky.

1.2 The inverse problem

We now assume, that the crack Σ is unknown, because it is completely hidden in the interior of Ω and hence not visible from outside. In order to detect the crack we consider measurements of both DIRICHLET data

$$u_m = u|_{\partial\Omega} \text{ (displacement field)} \quad \text{and} \quad \varphi_m = \varphi|_{\partial\Omega} \text{ (electric potential)}$$

on the outer boundary $\partial\Omega$, in addition to the known or just predefined NEUMANN data

$$F_m = \sigma(u,\varphi)\mathfrak{n}|_{\partial\Omega} \text{ (boundary stresses)} \quad \text{and} \quad g_m = D(u,\varphi)\cdot\mathfrak{n}|_{\partial\Omega} \text{ (boundary charges)}\,.$$

Note, that in the previously used notation $F_m = F$ and $g_m = g$. These overdetermined boundary data provide additional information, which will be used to gain information on the location of the crack, considering it as interior boundary part. Under the application of certain loads (F_m, g_m), at first, the normal vector and subsequently the exact position of the crack plane Π shall be determined. Π is defined by the plane equation $N\cdot x = c$ in the standard orthonormal system (O, e_1, e_2, e_3) with corresponding coordinate vectors $x = (x_1, x_2, x_3)^\top$; analogously the crack line in $\mathbb{R}^2$ is defined by omitting the 3rd coordinate. The inverse problem can be formulated as follows:

Problem 1 *Determine Σ such, that the solution of the differential equation (3) in the domain $\Omega\setminus\Sigma$ with the* NEUMANN *boundary conditions (4) and (5) or (6) leads to a displacement field u and an electric potential φ with $u = u_m$ and $\varphi = \varphi_m$ on $\partial\Omega$.*

1.3 Reciprocity principle and reciprocity gap

In order to construct a reciprocity gap functional like in [14] and combine the approaches of [2] and [1] for use in piezoelectricity, we consider an extension of the reciprocity principle to piezoelectric material behaviour.

Proposition 1 *Let $\Omega\subset\mathbb{R}^d$, $u, v\in[H^1(\Omega)]^d$, $\varphi,\psi\in H^1(\Omega)$. Furthermore, define the interdependence of $\sigma(u,\varphi)$ and $D(u,\varphi)$ by conditions (2) and in the matrix-vector-notation by (7), the same for u replaced by v and φ replaced by ψ. Then the following identity holds:*

$$\sigma(u,\varphi) : \varepsilon(v) + D(u,\varphi)\cdot\nabla\psi = \sigma(v,\psi) : \varepsilon(u) + D(v,\psi)\cdot\nabla\varphi\,. \tag{12}$$

Proof: We have $\underline{\underline{C}} = \underline{\underline{C}}^\top$, $\underline{\underline{K}} = \underline{\underline{K}}^\top \implies A = A^\top$. Hence,

$$\begin{aligned}\sigma(u,\varphi) : \varepsilon(v) + D(u,\varphi)\cdot\nabla\psi &\overset{(7)}{=} \begin{pmatrix}\underline{\varepsilon}(v)\\ \nabla\psi\end{pmatrix}^\top A \begin{pmatrix}\underline{\varepsilon}(u)\\ \nabla\varphi\end{pmatrix} = \begin{pmatrix}\underline{\varepsilon}(u)\\ \nabla\varphi\end{pmatrix}^\top A \begin{pmatrix}\underline{\varepsilon}(v)\\ \nabla\psi\end{pmatrix} \\ &= \sigma(v,\psi) : \varepsilon(u) + D(v,\psi)\cdot\nabla\varphi\,. \end{aligned}$$

□

Now we are going to formulate an extension of BETTI's reciprocity theorem to piezoelectric material in the case of divergence free stress fields and dielectric displacements.

Theorem 1 *Let Ω^* be a bounded domain with a sufficient smooth boundary (so that* Gauss*'s law is valid), Γ the complete boundary of Ω^* and n the outer normal on Γ. Define*

$$\mathbb{H} = \left\{(v,\psi) \in [H^1(\Omega^*)]^d \times H^1(\Omega^*) : \qquad \operatorname{div}\sigma(v,\psi) = \mathbf{0}\,,\ \operatorname{div} D(v,\psi) = 0 \quad \text{in } \Omega^*\right\}.$$

Then, for all $(u,\varphi)\,,\ (v,\psi) \in \mathbb{H}$ the following reciprocity relation holds:

$$\int_\Gamma (\sigma(u,\varphi)v + \psi D(u,\varphi)) \cdot n\, dS = \int_\Gamma (\sigma(v,\psi)u + \varphi D(v,\psi)) \cdot n\, dS\,.$$

Proof: First, we compute some divergences.

$$\begin{aligned} \operatorname{div}(\sigma(u,\varphi)v) &\overset{\sigma=\sigma^\top,(1)}{=} \underbrace{v \cdot \operatorname{div}\sigma(u,\varphi)}_{=0 \text{ for } (u,\varphi)\in\mathbb{H}} + \sigma(u,\varphi) : \varepsilon(v)\,, \\ \operatorname{div}(\psi D(u,\varphi)) &= \nabla\psi \cdot D(u,\varphi) + \underbrace{\psi \operatorname{div} D(u,\varphi)}_{=0 \text{ for } (u,\varphi)\in\mathbb{H}}\,. \end{aligned}$$

This enables to apply Gauss's law to prove the Theorem with the help of Proposition 1:

$$\begin{aligned} \int_\Gamma (\sigma(u,\varphi)v + \psi D(u,\varphi)) \cdot n\, dS &= \int_\Omega [\operatorname{div}(\sigma(u,\varphi)v) + \operatorname{div}(\psi D(u,\varphi))]\, dx \\ &= \int_\Omega [\sigma(u,\varphi) : \varepsilon(v) + \nabla\psi \cdot D(u,\varphi)]\, dx \\ &\overset{(12)}{=} \int_\Omega [\sigma(v,\psi) : \varepsilon(u) + \nabla\varphi \cdot D(v,\psi)]\, dx \\ &\overset{(v,\psi)\in\mathbb{H}}{=} \int_\Omega [\operatorname{div}(\sigma(v,\psi)u) + \operatorname{div}(\varphi D(v,\psi))]\, dx \\ &= \int_\Gamma (\sigma(v,\psi)u + \varphi D(v,\psi)) \cdot n\, dS \end{aligned}$$

□

We now introduce the space $\mathbb{H}$ with $\Omega^* = \Omega \setminus \Sigma$ and define the extended reciprocity gap functional. Let $(u,\varphi) \in \mathbb{H}$ be the solution of the problem (3),(4),(5) or (3),(4),(6) in the domain $\Omega \setminus \Sigma$. Then, for each pair of functions $(v,\psi) \in \mathbb{H}$ we define

$$RG(v,\psi) = \int_{\partial\Omega} [(\sigma(u,\varphi)v) - (\sigma(v,\psi)u) + \psi D(u,\varphi) - \varphi D(v,\psi)] \cdot \mathfrak{n}\, dS \tag{13}$$

$$= \int_{\partial\Omega} [F_m \cdot v - (\sigma(v,\psi)\mathfrak{n}) \cdot u_m + \psi g_m - \varphi_m D(v,\psi) \cdot \mathfrak{n}]\, dS\,. \tag{14}$$

Remark: *Due to the choice of $\mathbb{H}$, in a uncracked domain ($\Sigma = \emptyset$) the functional $RG(v,\psi)$ vanishes for each pair $(v,\psi) \in \mathbb{H}$ as a consequence of Theorem 1.*

However, if a crack exists, a reciprocity gap arises in the integral (13) because $\partial\Omega$ no longer represents the whole boundary of the domain $\Omega \setminus \Sigma$. The faces of Σ are additional parts of the boundary Γ.
Note that $\Omega \setminus \Sigma$ is a slit domain which does not fulfill the precondition on boundary smoothness of the Gaussian law (or Theorem 1) directly. But a commonly used method of domain splitting (see the proof of Lemma 1 below) allows to nevertheless use this identity and provides a connection between the arising gap in the functional $RG(.,.)$ and the unknown crack Σ.
Like in [15] at first proved under additional restrictions, one can show that – provided that traction free and impermeable (5) or semipermeable (6) boundary conditions are valid on the crack – the following merged extension of the corresponding Lemmas in [1] (also [14]) and [2] holds.

Lemma 1 *Let $\Omega \setminus \Sigma$ be a domain with a planar crack, $(u,\varphi) \in \mathbb{H}$ the solution of the boundary value problem (3),(4) with one of the conditions (5) or (6). With $\mathbb{H}_0 = \mathbb{H} \cap [\mathcal{C}(\Omega)]^{d+1}$ we have:*

$$RG(v,\psi) = \int_\Sigma [[\![u]\!] \cdot (\sigma(v,\psi)N) \; + \; [\![\varphi]\!](D(v,\psi)\cdot N)] \; ds \qquad \forall (v,\psi) \in \mathbb{H}_0\,. \tag{15}$$

Proof: We split Ω into two subdomains Ω^+ and Ω^- by the crack plane Π, see the illustration in figure 1.

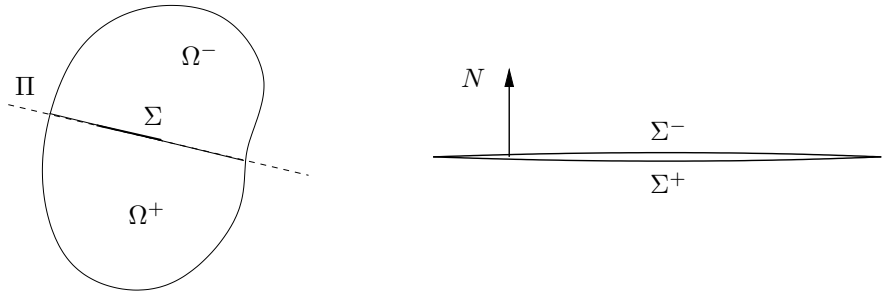

Figure 1: Splitting of the domain and crack (displayed as slightly opened) with N as outer normal to the crack face Σ^+ and inner normal to Σ^-

The boundaries of Ω^+ and Ω^- exhibit sufficient smoothness, hence Gauss's law holds in each part separately. W.l.o.g. we define N as normal to Π such that N is the outer normal of Ω^+. We denote by $\partial(\Omega^{+(-)})$ the complete boundary of $\Omega^{+(-)}$, furthermore

$$\Pi_o = \Pi \cap \Omega\,, \quad \partial\Omega_1 = \partial\Omega \cap \partial(\Omega^+)\,, \quad \partial\Omega_2 = \partial\Omega \cap \partial(\Omega^-)\,.$$

Then $\partial(\Omega^+) = \partial\Omega_1 \cup \Pi_o\,,\ \partial(\Omega^-) = \partial\Omega_2 \cup \Pi_o$. We can write

$$\begin{aligned}
RG(v,\psi) \;=\; & \underbrace{\int_{\partial(\Omega^+)} [\sigma(u,\varphi)v - \sigma(v,\psi)u \; + \; \psi D(u,\varphi) - \varphi D(v,\psi)]\cdot n\, dS}_{=0 \text{ (Theorem 1)}} \\
& - \int_{\Pi_o} \left[\sigma^+(u,\varphi)v - \sigma(v,\psi)u^+ \; + \; \psi D^+(u,\varphi) - \varphi^+ D(v,\psi)\right]\cdot N\, dS \\
& + \underbrace{\int_{\partial(\Omega^-)} [\sigma(u,\varphi)v - \sigma(v,\psi)u \; + \; \psi D(u,\varphi) - \varphi D(v,\psi)]\cdot n\, dS}_{=0 \text{ (Theorem 1)}} \\
& - \int_{\Pi_o} \left[\sigma^-(u,\varphi)v - \sigma(v,\psi)u^- \; + \; \psi D^-(u,\varphi) - \varphi^- D(v,\psi)\right]\cdot (-N)\, dS \\
=\; & \int_{\Pi_o} \big[\, \big(\sigma^-(u,\varphi) - \sigma^+(u,\varphi)\big)\, v + \sigma(v,\psi)(u^+ - u^-) \\
& \qquad + \psi\, \big(D^-(u,\varphi) - D^+(u,\varphi)\big) \; + \; (\varphi^+ - \varphi^-) D(v,\psi)\big]\cdot N\, dS\,.
\end{aligned}$$

Since the jumps of u, φ, σ and D vanish on $\Pi_o \setminus \Sigma$, we get

$$\begin{aligned}
RG(v,\psi) \;=\; & \int_\Sigma \left[\sigma(v,\psi)(u^+ - u^-) \; + \; (\varphi^+ - \varphi^-) D(v,\psi)\right]\cdot N\, dS \\
& + \int_\Sigma \underbrace{\big(\sigma^-(u,\varphi)N - \sigma^+(u,\varphi)N\big)}_{=0 \text{ due to (5) or (6)}} \cdot v\, dS \; + \; \int_\Sigma \psi\, \underbrace{\big(D^-(u,\varphi)\cdot N - D^+(u,\varphi)\cdot N\big)}_{=0 \text{ due to (5) or (6)}}\, dS \\
=\; & \int_\Sigma [\sigma(v,\psi)[\![u]\!] \; + \; [\![\varphi]\!] D(v,\psi)]\cdot N\, dS
\end{aligned}$$

□

Remarks:

- *The assumption of traction-free crack faces is used in the proof, but can be replaced by the more general condition*
$$\sigma^+(u,\varphi)N = \sigma^-(u,\varphi)N\,.$$
- *The continuous extension of* $[\![u]\!]$ *and* $[\![\varphi]\!]$ *by zero outside* Σ *to the whole plane* Π*, directly yields*
$$RG(v,\psi) = \int_{\Pi\cap\Omega} ([\![u]\!]\cdot(\sigma(v,\psi)N) + [\![\varphi]\!]D(v,\psi)\cdot N)\; dS\,.$$
- *In general, the computation of* $RG(.,.)$ *via (14) needs the complete elastic and electric* CAUCHY *data (*DIRICHLET- *and* NEUMANN-*) on the outer boundary. Certainly, the choice of special test functions and loads may allow a reduction of the necessary data.*

2 Identification of the crack normal

2.1 Methods of Identification

Two variants are possible to identify the crack normal, in each of them exactly one summand with jump vanishes in the integral of (15).

a) Identification by $[\![\varphi]\!]$
Choose affinely linear v^i, ψ^i (thus, automaticly $(v^i,\psi^i)\in\mathbb{H}$) with
$$D(v^i,\psi^i) = e_i\,, \qquad \sigma(v^i,\psi^i) = \mathbf{0}\,, \qquad i = 1,2(,3)\,.$$
Then the crack normal can be determined analogously to the pure electrostatic case (potential problem), as explained in [2]:
$$L_i = RG(v^i,\psi^i) = \int_\Sigma [\![\varphi]\!]N_i dS = N_i\int_\Sigma [\![\varphi]\!]dS\,.$$
Thus,
$$|L| = \sqrt{\sum_{i=1}^{d} RG^2(v^i,\psi^i)} = \left|\int_\Sigma [\![\varphi]\!]\,ds\right| \quad\Longrightarrow\; N_i = \frac{L_i}{|L|}\,.$$

b) Identification by $[\![u]\!]$
Choose affinely linear v^{ij}, ψ^{ij} with
$$D(v^{ij},\psi^{ij}) = \mathbf{0}\,, \qquad \sigma(v^{ij},\psi^{ij}) = E^{ij}\,, \qquad i,j = 1,2(,3)\,,$$
where $E^{ij}\in\mathbb{R}^{d,d}$ and $E^{ij}_{kl} = \frac{1}{2}\left(\delta^i_k\delta^j_l + \delta^i_l\delta^j_k\right)$.
In this case, a determination of the crack normal is possible analogously to the case of linear-elastic material behaviour as described in [1], [14].
We construct $R\in\mathbb{R}^{d,d}$ with $R_{ij} = RG(v^{ij},\psi^{ij})$. It can be shown (cf. Proposition 1 in [14]), that
$$R = \frac{1}{2}(N\mu^\top + \mu N^\top) \qquad \text{with } \mu = \int_\Sigma [\![u]\!]\,dS\,. \tag{16}$$
Furthermore, $\|\mu\|^2 = 2\|R\|_F^2 - (trR)^2$ and $\|\mu_n\|^2 = (\mu\cdot N)^2 = (trR)^2$, see Proposition 1 in [14]. Defining U as the normalized vector in the direction of μ, we have exactly $N+U$ and $N-U$ as eigenvectors to nonvanishing eigenvalues of R (except for the special case

$U = \pm N$, where only one nonvanishing eigenvalue exists). Hence, N can be determined by computing $R^{(1)}$ and $R^{(2)}$ with two different loads, which lead to $U^{(1)} \neq U^{(2)}$ while N remains unchanged.

We point to Section 2.3 for a stability analysis of this procedure.

Due to the choice of the test functions, in variant a) the summand $(\sigma(v,\psi)\cdot\mathfrak{n})\cdot u$ vanishes in the reciprocity integral (13), where in variant b) the summand $(D(v,\psi)\cdot\mathfrak{n})\cdot\phi$ vanishes. So, one type of DIRICHLET data is dispensable. It is not possible to avoid the more difficult measurement of the NEUMANN data $\sigma(u,\varphi)\cdot\mathfrak{n}$ on $\partial\Omega$ using this kind of test functions. This might be achievable by fixing boundary forces.
To evaluate the boundary integral, we also need the values of v and ψ on $\partial\Omega$. We first use the inverse material law to compute $\varepsilon(v)$, $\nabla\psi$

$$\begin{pmatrix} \underline{\varepsilon}(v) \\ \nabla\psi \end{pmatrix} = A^{-1} \begin{pmatrix} \underline{\sigma}(v,\psi) \\ D(v,\psi) \end{pmatrix} . \tag{17}$$

and then obtain the desired primary fields by integration. The inverse material matrix has the same block structure as the direct one in (7), we denote

$$A^{-1} = \begin{pmatrix} \mathfrak{A} & \mathfrak{B} \\ \mathfrak{B}^\top & -\mathfrak{D} \end{pmatrix} .$$

The pattern of nonzeros of the matrix blocks is also analogous. In the two-dimensional case one obtains by translation formulas from [12] or [13] the constant entries of the matrices

$$\mathfrak{A} = \begin{pmatrix} a_{11} & a_{12} & 0 \\ a_{12} & a_{22} & 0 \\ 0 & 0 & a_{33} \end{pmatrix} , \ \mathfrak{B} = \begin{pmatrix} 0 & b_{12} \\ 0 & b_{22} \\ b_{31} & 0 \end{pmatrix} , \ \mathfrak{D} = \begin{pmatrix} \delta_{11} & 0 \\ 0 & \delta_{22} \end{pmatrix} .$$

2.2 Explicit representation of the test fields in the two-dimensional case

In variant a) we have $D(v^1,\psi^1) = (1,0)^\top$, $D(v^2,\psi^2) = (0,1)^\top$ and obtain from the inverse material law:

$$\underline{\varepsilon}(v^1) = \begin{pmatrix} 0 \\ 0 \\ b_{31} \end{pmatrix} , \quad \underline{\varepsilon}(v^2) = \begin{pmatrix} b_{12} \\ b_{22} \\ 0 \end{pmatrix} , \quad \nabla\psi^1 = -\begin{pmatrix} \delta_{11} \\ 0 \end{pmatrix} , \quad \nabla\psi^2 = -\begin{pmatrix} 0 \\ \delta_{22} \end{pmatrix} .$$

Possible test functions are:

$$v^1 = \frac{b_{31}}{2}\begin{pmatrix} x_2 \\ x_1 \end{pmatrix} , \quad v^2 = \begin{pmatrix} b_{12}x_1 \\ b_{22}x_2 \end{pmatrix} , \quad \psi^1 = -\delta_{11}x_1 , \quad \psi^2 = -\delta_{22}x_2 .$$

In variant b) we have
$\underline{\sigma}(v^{11},\psi^{11}) = (1,0,0)^\top$, $\underline{\sigma}(v^{22},\psi^{22}) = (0,1,0)^\top$ and $\underline{\sigma}(v^{11},\psi^{11}) = (0,0,\frac{1}{2})^\top$. Thus,

$$\underline{\varepsilon}(v^{11}) = \begin{pmatrix} a_{11} \\ a_{12} \\ 0 \end{pmatrix} , \quad \underline{\varepsilon}(v^{22}) = \begin{pmatrix} a_{12} \\ a_{22} \\ 0 \end{pmatrix} , \quad \underline{\varepsilon}(v^{12}) = \frac{1}{2}\begin{pmatrix} 0 \\ 0 \\ a_{33} \end{pmatrix} ,$$

$$\nabla\psi^{11} = \begin{pmatrix} 0 \\ b_{12} \end{pmatrix} , \quad \nabla\psi^{22} = \begin{pmatrix} 0 \\ b_{22} \end{pmatrix} , \quad \nabla\psi^{12} = \frac{1}{2}\begin{pmatrix} b_{31} \\ 0 \end{pmatrix} ,$$

and the corresponding test functions:

$$v^{11} = \begin{pmatrix} a_{11}x_1 \\ a_{12}x_2 \end{pmatrix} , \ v^{22} = \begin{pmatrix} a_{12}x_1 \\ a_{22}x_2 \end{pmatrix} , \ v^{12} = \frac{a_{33}}{4}\begin{pmatrix} x_2 \\ x_1 \end{pmatrix} , \quad \psi^{11} = b_{12}x_2 , \ \psi^2 = b_{22}x_2 , \ \psi^{12} = \frac{b_{31}}{2}x_1 .$$

2.3 Stability

Since the given measurements F_m^δ, u_m^δ of F_m, u_m are actually contaminated by noise, we have to make sure that small perturbations in the data only lead to small perturbations in the reconstructed crack. We here mainly investigate the method for crack normal determination based on the displacement jump, i.e., b) in Subsection 2.1, since this involves computation of eigenvectors. The reconstruction of N relies on the fact that the measured matrix of reciprocity gap values $R_{ij} = RG(v^{ij}, \psi^{ij})$ lies in the set

$$\mathcal{M} = \{\frac{1}{2}(ab^\top + ba^\top) \ : \ a, b \in \mathbb{R}^d, \|a\| = 1\} = \{\frac{1}{2}(ab^\top + ba^\top) \ : \ a, b \in \mathbb{R}^d\} \tag{18}$$

where $d \in \{2, 3\}$, that can be characterized as follows:

Lemma 2 *For the set $\mathcal{M}$ as defined in* (18) *we have the identity*

$$\mathcal{M} = \widetilde{\mathcal{M}} := \{R \in \mathbb{R}^{d\times d} \ : \ (trR)^2 \le \|R\|_F^2 \ \wedge \ rank(R) \le 2 \ \wedge \ R = R^\top\}$$

Proof. The fact that $\mathcal{M} \subseteq \widetilde{\mathcal{M}}$ is readily checked by just computing the Frobenius norm (using $\|R\|_F^2 = tr(R^\top R)$) and trace of a matrix of the form given in (18):

$$\begin{aligned} &\|\frac{1}{2}(ab^\top + ba^\top)\|_F^2 - \left[tr(\frac{1}{2}(ab^\top + ba^\top))\right]^2 \\ &= \ \frac{1}{4}tr((ab^\top + ba^\top)^2) - \left[\frac{1}{2}tr(ab^\top + ba^\top)\right]^2 = \frac{1}{2}(\|a\|^2\|b\|^2 - (a^\top b)^2) \ge 0 \end{aligned}$$

where we have used the elementary identity $tr(ab^\top) = a^\top b$ and the Cauchy-Schwarz inequality. On the other hand, given an arbitraty $R \in \widetilde{\mathcal{M}}$ we set

$$\bar{R} = \frac{R}{\sqrt{2\|R\|_F^2 - (trR)^2}}\,,$$

where the expression under the square root is larger or equal to $\|R\|_F^2$. Abbreviating $\alpha = tr\bar{R}$ and noting that $\alpha^2 \le 1$ by $R \in \widetilde{\mathcal{M}}$, we now verify that the eigenvalues of $\bar{R}$ are given by

$$\lambda_1 = \frac{\alpha + 1}{2}\,, \quad \lambda_2 = \frac{\alpha - 1}{2}\,, \quad (\lambda_3 = 0 \text{ if } d = 3)\,. \tag{19}$$

(cf. Proposition 2 in [14]). Existence of a vanishing eigenvalue $\lambda_3 = 0$ in case $d = 3$ immediately follows from the fact that $\mathrm{rank}(\bar{R}) = \mathrm{rank}(R) \le 2$. From the identities

$$\begin{aligned} \|\bar{R}\|_F^2 &= \lambda_1^2 + \lambda_2^2 + \lambda_3^2 = \lambda_1^2 + \lambda_2^2 \\ \|\bar{R}\|_F^2 &= \frac{\|R\|_F^2}{2\|R\|_F^2 - (trR)^2} = \frac{1}{2}(1 + \alpha^2) \\ \alpha &= tr\bar{R} = \lambda_1 + \lambda_2 + \lambda_3 = \lambda_1 + \lambda_2\,, \text{ i.e., } \lambda_2 = \alpha - \lambda_1 \end{aligned}$$

we can easily extract the quadratic equation

$$\lambda_1^2 - \alpha\lambda_1 + \frac{1}{4}\alpha^2 - \frac{1}{4} = 0\,,$$

which yields $\lambda_1 = \frac{1}{2}(\alpha \pm 1)$, $\lambda_2 = \alpha - \lambda_1 = \frac{1}{2}(\alpha \mp 1)$, i.e., (19). Denoting by Φ_i a normalized eigenvector for λ_i, $i = 1, 2$ and setting

$$z_1 = \sqrt{2(1+\alpha)}\Phi_1\,, \ z_2 = \sqrt{2(1-\alpha)}\Phi_2\,, \ a = \frac{z_1 + z_2}{2}\,, \ b = \frac{z_1 - z_2}{2}\,, \tag{20}$$

(cf. Subsection 3.3 in [14]) we obtain

$$\frac{1}{2}(ab^\top + ba^\top) = \frac{1}{4}(z_1 z_1^\top - z_2 z_2^\top) = \frac{1+\alpha}{2}\Phi_1\Phi_1^\top - \frac{1-\alpha}{2}\Phi_2\Phi_2^\top = \sum_{i=1}^{d}\lambda_i\Phi_i\Phi_i^\top = \bar{R}\,.$$

□

It can be shown (cf. Proposition 1 in [14]) that the exactly measured matrix entries lead to a matrix R that is contained in $\mathcal{M}$, see (16). However, even arbitrarily small perturbartions may lead to a violation of the identity in (16). We therefore have to map the measured data into the set $\mathcal{M}$ before applying the procedure sketched in item b) of Subsection 2.1. Note that plain metric projection is not an option, since $\mathcal{M}$ is not convex as the following simple counterexample shows: Choose $c, f \in \mathbb{R}^d$ with $c^\top f = 0$, $c \neq 0$, $f \neq 0$. Then obviously $cc^\top$ and $ff^\top$ are both elements of $\mathcal{M}$, but $\frac{1}{2}(cc^\top + ff^\top)$ is not, since the identity

$$\frac{1}{2}(cc^\top + ff^\top) = \frac{1}{2}(ab^\top + ba^\top)$$

by multiplication with c and f, from the left and right hand side, respectively, leads to a contradiction:

$$\begin{aligned}
\|c\|^4 &= 2(a^\top c)(b^\top c) \quad \Rightarrow\ (a^\top c) \neq 0\ \wedge\ (b^\top c) = \frac{\|c\|^4}{2(a^\top c)} \\
\|f\|^4 &= 2(a^\top f)(b^\top f) \quad \Rightarrow\ (b^\top f) \neq 0\ \wedge\ (a^\top f) = \frac{\|f\|^4}{2(b^\top f)} \\
0 &= (a^\top c)(b^\top f) + (a^\top f)(b^\top c) = (a^\top c)(b^\top f)\left(1 + \frac{\|c\|^4\|f\|^4}{4(a^\top c)^2(b^\top f)^2}\right) \neq 0\,.
\end{aligned}$$

Thus we propose an alternative strategy to construct, for a given R^δ with

$$\|R^\delta - R\|_F \leq \delta\,,$$

which is obviously satisfied for

$$\delta^2 = \sum_{i,j=1}^{d}\|v^{ij}\|^2_{L^q(\partial\Omega)}\|F_m^\delta - F_m\|^2_{L^p(\partial\Omega)} + \sum_{i,j=1}^{d}\|E^{ij}\mathfrak{n}\|^2\mathrm{meas}(\partial\Omega)^{2/q}\|u_m^\delta - u_m\|^2_{L^p(\partial\Omega)}\,,$$

where $\frac{1}{p} + \frac{1}{q} = 1$, a nearby $\tilde{R}^\delta \in \mathcal{M}$. Only the upper (lower) triangular part of R^δ is actually computed, the rest of the matrix is completed in a symmetric manner, hence R^δ is symmetric. We subtract a sufficiently large quantity from the diagonal, i.e.

$$\tilde{R}^\delta = R^\delta - \frac{\zeta}{d}I$$

with

$$\zeta \in [\zeta_-, \zeta_+]\,, \quad \zeta_\pm = \hat{\alpha} \pm \sqrt{\frac{d}{d-1}(\|R^\delta\|_F^2 - \frac{1}{d}\hat{\alpha}^2)}\,,$$

where we abbreviate $\hat{\alpha} = trR^\delta$. Therewith we obtain

$$\begin{aligned}
(tr\tilde{R}^\delta)^2 &= \hat{\alpha}^2 - 2\hat{\alpha}\zeta + \zeta^2 = \underbrace{\frac{d-1}{d}\zeta^2 - 2\frac{d-1}{d}\hat{\alpha}\zeta + \hat{\alpha}^2 - \|R^\delta\|_F^2}_{=\frac{d-1}{d}(\zeta-\zeta_-)(\zeta-\zeta_+)} + \|R^\delta\|_F^2 + \frac{\zeta^2}{d} - 2\frac{\hat{\alpha}\zeta}{d} \\
&\leq \|R^\delta\|_F^2 + \frac{\zeta^2}{d} - 2\frac{\hat{\alpha}\zeta}{d} = \|\tilde{R}^\delta\|_F^2\,.
\end{aligned}$$

On the other hand, ζ should be chosen sufficiently small, namely in case $\|R^\delta\|_F^2 \geq \hat{\alpha}^2$ we can set $\zeta = 0$ and in case $\|R^\delta\|_F^2 < \hat{\alpha}^2$ we set $\zeta = \zeta_-$ with

$$\begin{aligned} 0 &\leq \zeta_- = \hat{\alpha} - \sqrt{\hat{\alpha}^2 - \frac{d}{d-1}(\hat{\alpha}^2 - \|R^\delta\|_F^2)} \\ &= \frac{d}{d-1} \frac{\hat{\alpha}^2 - \|R^\delta\|_F^2}{\hat{\alpha} + \sqrt{\hat{\alpha}^2 - \frac{d}{d-1}(\hat{\alpha}^2 - \|R^\delta\|_F^2)}} \\ &\leq \frac{d}{d-1} \frac{\hat{\alpha}^2 - \|R^\delta\|_F^2}{\hat{\alpha}} \leq \frac{d}{d-1} \frac{\hat{\alpha}^2 - \|R^\delta\|_F^2}{\|R^\delta\|_F}, \end{aligned}$$

where by $R \in \mathcal{M}$

$$\hat{\alpha}^2 - \|R^\delta\|_F^2 = (trR)^2 - \|R\|_F^2 + [(trR^\delta)^2 - (trR)^2] + [\|R\|_F^2 - \|R^\delta\|_F^2] \leq [(trR^\delta)^2 - (trR)^2] + [\|R\|_F^2 - \|R^\delta\|_F^2],$$

hence altogether there exists a $\bar{\delta} > 0$ such that for all $\delta \in (0, \bar{\delta}]$ we have $|\zeta| \leq \hat{C}\delta$ for some $\hat{C} > 0$ and therewith

$$\|\tilde{R}^\delta - R\| \leq \bar{C}\delta \tag{21}$$

for some constant $\bar{C}$ depending only on $\|R\|_F$ and trR.

In remains to investigate stability of the procedure of finding a, b such that $\tilde{R}^\delta = \frac{1}{2}(ab^\top + ba^\top)$ as described in the proof of Lemma 2 and as used in the construction of N according to item b) in Subsection 2.1, see also [14] for more details. For this purpose consider $R = (R_{ij})_{ij \in \{1,2,3\}}$ (i.e., we omit the tilde and the superscript δ in the matrix entries). It is readily checked that an eigenvector corresponding to $\lambda_i = \frac{\alpha \pm 1}{2}$ is given by

$$\check{\Phi}_i := \begin{pmatrix} R_{12}R_{23} - D_2^\pm R_{13} \\ R_{12}R_{13} - D_1^\pm R_{23} \\ D_1^\pm D_2^\pm - R_{12}^2 \end{pmatrix}, \quad i = 1, 2, \tag{22}$$

where $D_k^\pm = \frac{R_{kk} - R_{[k+1][k+1]} - R_{[k+2][k+2]} \mp 1}{2}$, $[j] = (j-1)_{\mathrm{mod}\ 3} + 1$, in case $d = 3$ and by

$$\check{\Phi}_i := \begin{pmatrix} -R_{12} \\ \frac{R_{11} - R_{22} \mp 1}{2} \end{pmatrix}, \quad i = 1, 2, \tag{23}$$

in case $d = 2$. Moreover,

$$\check{\Phi}_3 := \begin{pmatrix} R_{12}R_{23} - R_{22}R_{13} \\ R_{12}R_{13} - R_{11}R_{23} \\ R_{11}R_{22} - R_{12}^2 \end{pmatrix} \tag{24}$$

is an eigenvector corresponding to the eigenvalue $\lambda = 0$ in case $d = 3$. Computation of these vectors obviously depends in a Lipschitz stable manner on the matrix entries. The same holds for the computation of the norms of these vectors. Hence, unless $\|\check{\Phi}_i\|$ vanishes, defining $\check{\Phi}_i^\delta$ as the vectors defined in (22), (23), (24) with R_{ij} replaced by $\tilde{R}_{ij}^\delta$, we get, for $\Phi_i^{(\delta)} = \frac{\check{\Phi}_i^{(\delta)}}{\|\check{\Phi}_i^{(\delta)}\|}$ the stability estimate

$$\|\Phi_i^\delta - \Phi_i\| \leq c\delta$$

for some constant c depending only on $\|\Phi_i\|$. The problem of vanishing norm $\|\check{\Phi}_i\|$ can be circumvented by using alternative eigenvector representations (that have to be collinear to $\check{\Phi}_i^\delta$ since the eigenspace must have dimension one) such as

$$\bar{\Phi}_i^\delta = \begin{pmatrix} D_2^{\pm\delta} D_3^{\pm\delta} - {R_{23}^\delta}^2 \\ R_{13}^\delta R_{23}^\delta - D_3^{\pm\delta} R_{12}^\delta \\ R_{12}^\delta R_{23}^\delta - D_2^{\pm\delta} R_{13}^\delta \end{pmatrix} \text{ or } \bar{\Phi}_i^\delta = \begin{pmatrix} R_{13}^\delta R_{23}^\delta - D_3^{\pm\delta} R_{12}^\delta \\ D_1^{\pm\delta} D_3^{\pm\delta} - {R_{13}^\delta}^2 \\ R_{12}^\delta R_{13}^\delta - D_1^{\pm\delta} R_{23}^\delta \end{pmatrix}, \quad i = 1, 2 \text{ in 3D}$$

$$\bar{\Phi}_i^\delta = \begin{pmatrix} \frac{R_{22}-R_{11}\mp 1}{2} \\ -R_{12} \end{pmatrix}, \quad i = 1,2 \text{ in 2D} \tag{25}$$

in case $\|\check{\Phi}_i^\delta\| \leq \bar{C}\delta$ with $\bar{C}$ as in (21) (so that $\|\check{\Phi}_i\|$ potentially vanishes). It can be shown that not all of these eigenvalue representations vanish simultaneously, so that we can always select a stable representation. We demonstrate this in the $2d$ case: If $\|\check{\Phi}_i^\delta\| \leq \bar{C}\delta$ then we have

$$\begin{aligned}
\|\bar{\Phi}_i^\delta\|^2 &= R_{12}^2 + \frac{(R_{22}-R_{11}\mp 1)^2}{4} \\
&= \|\check{\Phi}^\delta\|^2 + \frac{(R_{22}-R_{11}\mp 1)^2 - (R_{11}-R_{22}\mp 1)^2}{4} \\
&= \|\check{\Phi}^\delta\|^2 + \frac{((R_{22}-R_{11}\mp 1)+(R_{11}-R_{22}\mp 1))((R_{22}-R_{11}\mp 1)-(R_{11}-R_{22}\mp 1))}{4} \\
&= \|\check{\Phi}^\delta\|^2 + \frac{(\mp 2)2(R_{22}-R_{11})}{4} \\
&= \|\check{\Phi}^\delta\|^2 + 1 \pm (R_{11}-R_{22}\mp 1) \\
&\geq 1 - \bar{C}\delta \geq \frac{1}{2}
\end{aligned}$$

for all $\delta \in (0, \min\{\frac{1}{2\bar{C}}, \bar{\delta}\}]$.
The remaining computations according to (20) are obviously again Lipschitz stable, so that for the normal $N = \frac{a}{\|a\|}$ or $N = \frac{b}{\|b\|}$ we end up with an overall estimate

$$\|N^\delta - N\| \leq \overline{C}\delta$$

for all $\delta \in (0, \overline{\delta}]$ with some sufficiently small $\overline{\delta}$ and some constant $\overline{C}$ independent of δ.

3 Determination of the crack plane or -line Π

In order to reconstruct the crack plane it remains to determine the distance to the origin. For this purpose we can again choose between an approach using purely electric or purely mechanical measurements, respectively.

3.1 Variants for determining the plane offset

Having obtained the crack normal N according to Section 2 we can – like in the electrostatic or in the anisotropic-elastic case – generate a new coordinate system containing the crack normal N as a coordinate direction. Let the new coordinate system be denoted by (O', T, V, N) in $\mathbb{R}^3$ or (O', T, N) in $\mathbb{R}^2$, respectively, with corresponding coordinates X_k, and the origin positioned outside the domain Ω in order to obtain uniqueness of the sign of C. In these new coordinates, the equation for the crack plane (or crack line) is defined by $X_d = C$, $d \in \{2,3\}$ and the crack normal has the representation $N = (0,(0,)1)^\top$.
Our aim is now to construct appropriate test functions v and ψ in the context of the coupled material law, in order to compute C from the value $RG(v,\psi)$ using Lemma 1. For this purpose, correspondingly to the crack normal determination, we propose two approaches, that we describe only in 2D for simplicity of exposition.

a) Determination via $[\![\varphi]\!]$
Choose $(v_E, \psi_E) \in \mathbb{H}$ with

$$D(v_E,\psi_E)\cdot N = X_2\,, \qquad \sigma(v_E,\psi_E)\cdot N = \mathbf{0}\,. \tag{26}$$

Inserting into equation (15) of Lemma 1 we obtain

$$RG(v_E,\psi_E) = \int_\Sigma [\![\varphi]\!]\cdot X_2\, dS = C\int_\Sigma [\![\varphi]\!]\, ds\,.$$

Analogously to the electrostatic case [2] we can now determine C by means of the reciprocity integrals already computed for determination of the crack normal (cf. Section 2) as follows:

$$C = \frac{|RG(v_E, \psi_E)|}{\sqrt{RG^2(v^1, \psi^1) + RG^2(v^2, \psi^2)}}\,.$$

b) Determination via $[\![u]\!]$
Choose $(v_T, \psi_T) \in \mathbb{H}$ with

$$D(v_T, \psi_T) \cdot N = 0\,, \qquad \sigma(v_T, \psi_T) \cdot N = \begin{pmatrix} X_2 \\ 0 \end{pmatrix}\,. \tag{27}$$

Inserting into equation (15) of Lemma 1 we here arrive at

$$RG(v_T, \psi_T) = \int_\Sigma [\![u_T]\!] \cdot X_2 \, dS \; = C \int_\Sigma [\![u_T]\!] \, dS$$

with the possibility of determining C like in the purely elastic case ([1], [14]):

$$C = \frac{|RG(v_T, \psi_T)|}{\sqrt{2(\|R\|_F^2 - (trR)^2)}}\,. \tag{28}$$

3.2 Material law in rotated coordinates

For the transformation into the new coordinate system we have to perform a rotation. Due to the anisotropy, the material law changes in dependence of the rotation angle (like in the linear elastic case). Except for the material matrices, we mark values in the original coordinate system (x-coordinates) with a tilde, to distinguish from the notation in X-coordinates in the coordinate system aligned to the crack normal.
As introduced in [14] we define the matrices $P(\phi)$ and $Q(\phi)$ as

$$Q(\phi) = \begin{pmatrix} \cos\phi & 0 & \sin\phi \\ 0 & 1 & 0 \\ -\sin\phi & 0 & \cos\phi \end{pmatrix},\; P(\phi) = \begin{pmatrix} \cos^2\phi & 0 & \sin^2\phi & 0 & \cos\phi\sin\phi & 0 \\ 0 & 1 & 0 & 0 & 0 & 0 \\ \sin^2\phi & 0 & \cos^2\phi & 0 & -\cos\phi\sin\phi & 0 \\ 0 & 0 & 0 & \cos\phi & 0 & -\sin\phi \\ -2\cos\phi\sin\phi & 0 & 2\cos\phi\sin\phi & 0 & \cos^2\phi - \sin^2\phi & 0 \\ 0 & 0 & 0 & \sin\phi & 0 & \cos\phi \end{pmatrix}$$

in 3D,

$$Q(\phi) = \begin{pmatrix} \cos\phi & \sin\phi \\ -\sin\phi & \cos\phi \end{pmatrix},\; P(\phi) = \begin{pmatrix} \cos^2\phi & \sin^2\phi & \cos\phi\sin\phi \\ \sin^2\phi & \cos^2\phi & -\cos\phi\sin\phi \\ -2\cos\phi\sin\phi & 2\cos\phi\sin\phi & \cos^2\phi - \sin^2\phi \end{pmatrix} \quad \text{in 2D.}$$

In extension to the linear elastic case we obtain

$$\tilde{\underline{\varepsilon}}(\tilde{u}) = P(\phi)\,\underline{\varepsilon}(u)\,, \qquad \tilde{\nabla}\varphi = Q(\phi)\nabla\varphi\,.$$

From (7) the material law in the new coordinates follows:

$$\begin{pmatrix} \underline{\sigma}(u,\varphi) \\ D(u,\varphi) \end{pmatrix} = \begin{pmatrix} P^\top(\phi) & \\ & Q^\top(\phi) \end{pmatrix} \begin{pmatrix} \underline{\underline{C}} & \underline{\underline{B}} \\ \underline{\underline{B}}^\top & -\underline{\underline{K}} \end{pmatrix} \begin{pmatrix} P(\phi) & \\ & Q(\phi) \end{pmatrix} \begin{pmatrix} \underline{\varepsilon}(u) \\ \nabla\varphi \end{pmatrix}\,. \tag{29}$$

The inverse material law results as

$$\begin{pmatrix} \underline{\varepsilon}(u) \\ \nabla\varphi \end{pmatrix} = \begin{pmatrix} P(-\phi) & \\ & Q(-\phi) \end{pmatrix} \begin{pmatrix} \mathfrak{A} & \mathfrak{B} \\ \mathfrak{B}^\top & -\mathfrak{D} \end{pmatrix} \begin{pmatrix} P^\top(-\phi) & \\ & Q^\top(-\phi) \end{pmatrix} \begin{pmatrix} \underline{\sigma}(u,\varphi) \\ D(u,\varphi) \end{pmatrix}\,.$$

3.3 Choice of appropriate test fields

Here our aim is to find test functions in $\mathbb{H}$ that satisfy equation (26) in case of method a) or equation (27) in case of method b), respectively.

Variant a) With divergence free dielectric displacement

$$D(v,\psi) = \begin{pmatrix} -X_1 \\ X_2 \end{pmatrix}$$

like in the electrostatic case and vanishing stress $\sigma(v,\psi)$, the inverse material law would yield

$$\underline{\varepsilon}(v) = P(-\phi)\mathfrak{B}Q^\top(-\phi)D(v,\psi)\,, \qquad \nabla\psi = -Q(-\phi)\mathfrak{D}Q^\top(-\phi)D(v,\psi)\,.$$

While it is always possible to construct a displacement field v corresponding to $\underline{\varepsilon}(v)$, a gradient field has to satisfy the integrability condition. With the notation $Q(-\phi)\mathfrak{D}Q^\top(-\phi) = (d_{ij})$, the expression

$$\nabla\psi = \begin{pmatrix} d_{11}X_1 - d_{12}X_2 \\ d_{12}X_1 - d_{22}X_2 \end{pmatrix}$$

with $d_{12} = (\delta_{11} - \delta_{22})\cos\phi\sin\phi$ for general angle ϕ only defines a gradient field if $d_{12} = -d_{12} = 0$ holds. However, in anisotropic material this is violated, since in general $\delta_{11} \neq \delta_{22}$.
This problem can be solved by adding divergence free terms:

$$D(v_E,\psi_E) = \begin{pmatrix} -X_1 + \gamma_E X_2 \\ X_2 \end{pmatrix}, \quad \sigma(v_E,\psi_E) = \mathbf{0}$$

or

$$D(v_E,\psi_E) = \begin{pmatrix} -X_1 \\ X_2 \end{pmatrix}, \quad \sigma(v_E,\psi_E) = \gamma_{E,\sigma}\begin{pmatrix} X_2 & 0 \\ 0 & 0 \end{pmatrix}.$$

The integrability condition yields

$$\begin{aligned} \gamma_E &= -2\frac{d_{12}}{d_{11}} = 2\frac{(\delta_{22}-\delta_{11})\cos\phi\sin\phi}{\delta_{11}\cos^2\phi + \delta_{22}\sin^2\phi}\,, \\ \gamma_{E,\sigma} &= 2\frac{d_{12}}{(1,0)Q(-\phi)\mathfrak{B}^\top P^\top(-\phi)(1,0,0)^\top} = 2\frac{(\delta_{22}-\delta_{11})\cos\phi}{(b_{31}+b_{12})\cos^2\phi + b_{22}\sin^2\phi}\,. \end{aligned}$$

Variant b) The choice

$$D(v,\psi) = \mathbf{0}\,, \qquad \sigma(v,\psi) = \begin{pmatrix} -X_1 & X_2 \\ X_2 & 0 \end{pmatrix}$$

via the inverse material law in general does not lead to a gradient field $\nabla\psi$ either.
Similarly to variant a) we therefore choose

$$D(v_T,\psi_T) = \gamma_T\begin{pmatrix} X_2 \\ 0 \end{pmatrix}, \quad \sigma(v,\psi) = \begin{pmatrix} -X_1 & X_2 \\ X_2 & 0 \end{pmatrix}$$

or

$$D(v_T,\psi_T) = \mathbf{0}, \quad \sigma(v,\psi) = \begin{pmatrix} -X_1 & X_2 \\ X_2 & 0 \end{pmatrix} + \gamma_{T,\sigma}\begin{pmatrix} X_2 & 0 \\ 0 & 0 \end{pmatrix}$$

and by inserting into the intagrability condition get the parameter γ_T or $\gamma_{T,\sigma}$, respectively.
By integration we finally obtain test fields for displacement and potential in both cases.

4 Approximative mid point determination of a single crack

Nearly the same idea as in Section 3 can be used to find the center of the crack in a certain sense. Using the introduced new coordinates with the (possibly again moved) orign s.t. $\forall X \in \Omega : X_i \geq 0,\ 1 \leq i \leq d$, it remains to find $X_i\,,\ 1 \leq i \leq d-1$. Again we evaluate $RG(v,\psi)$ for some appropriate test functions in two variants:

a) Use of $[\![\varphi]\!]$
For $1 \leq i \leq d-1$ choose $(v_{M,i}, \psi_{M,i}) \in \mathbb{H}$ with

$$D(v_{M,i},\psi_{M,i})\cdot N = X_i\,, \quad \sigma(v_{M,i},\psi_{M,i})\cdot N = \mathbf{0} \quad \overset{\text{Lemma 1}}{\Longrightarrow} \quad RG(v_{M,i},\psi_{M,i}) = \int_\Sigma [\![\varphi]\!]\cdot X_2\, dS\,. \tag{30}$$

Hence, using $|L|$ from Section 2 we define the point $\xi \in \Pi$ with

$$\xi_d = C\,, \quad \xi_i = \frac{|RG(v_{M,i},\psi_{M,i})|}{|L|} \text{ for } 1 \leq i \leq d-1\,.$$

b) Use of $[\![u]\!]$
For $1 \leq i \leq d-1$ choose $(v_{m,i}, \psi_{m,i}) \in \mathbb{H}$ with

$$D(v_{m,i},\psi_{m,i})\cdot N = 0\,, \qquad \sigma(v_{m,i},\psi_{m,i})\cdot N = X_i\, e_d\,. \tag{31}$$

Here, with the matrix R from Section 2 and $\|\mu_n\| = |trR|$ we get ξ with

$$\xi_i = \frac{|RG(v_{M,i})|}{|trR|},\ 1 \leq i \leq d-1\,.$$

In both cases it can be shown, that ξ is in the convex hull of Σ. In the case of a convex single crack with nearly symmetric behaviour of the potential jump (a) or of the normal displacement jump (b), ξ gives a good approximation for the center of Σ (or just the mid point when $d = 2$).

Choice of test fields

As in Section 3, admissible test functions require the gradient property of $\nabla\psi$. We ensure this by adding X_d-parts to $D(v,\psi)$. In the twodimensional case this leads to ($i = 1$ omitted):

$$D(v_M,\psi_M) = \begin{pmatrix}\gamma_{cE}X_2\\ X_1\end{pmatrix}, \quad \sigma(v_E,\psi_E) = \mathbf{0} \qquad \text{with } \gamma_{cE} = \frac{\delta_{11}\sin^2\phi + \delta_{22}\cos^2\phi}{\delta_{11}\cos^2\phi + \delta_{22}\sin^2\phi}\,,$$

$$D(v_m,\psi_m) = \begin{pmatrix}\gamma_{cT}X_2\\ 0\end{pmatrix}, \quad \sigma(v_E,\psi_E) = \begin{pmatrix}0 & 0\\ 0 & X_1\end{pmatrix} \qquad \text{with } \gamma_{cT} = -\frac{\cos\phi\left((b_{12}+b_{31})\sin^2\phi + b_{22}\cos^2\phi\right)}{\delta_{11}\cos^2\phi + \delta_{22}\sin^2\phi}\,.$$

5 Numerical 2D-examples

5.1 Setup of examples

In extension to the purely elastic setting in [14], we consider test problems with piezoelectric material behaviour.
For this purpose we use the full material parameter set of the ceramic PZT4$_b$, as can be found, e.g., in [11] or [12]. As boundary conditions on the crack we will impose vanishing normal stresses and electric impermeability (5).
The computational domain will be $\Omega = [0,8]\times[0,2]$ in the first example, $\Omega = [0,4]^2$ in the second example. The polarization is in x_2-direction in all tests.
In example 1 we deal with a horizontal crack which is splitted unsymmetrically in two parts, and the purely mechanical loads displayed in Fig. 2 are investigated, i.e., $g_m = 0$ on $\partial\Omega$.

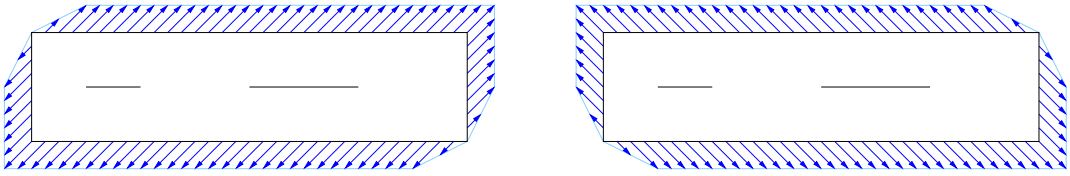

Figure 2: Illustration of the loads $F_m^{(1)}$ and $F_m^{(2)}$ in example 1

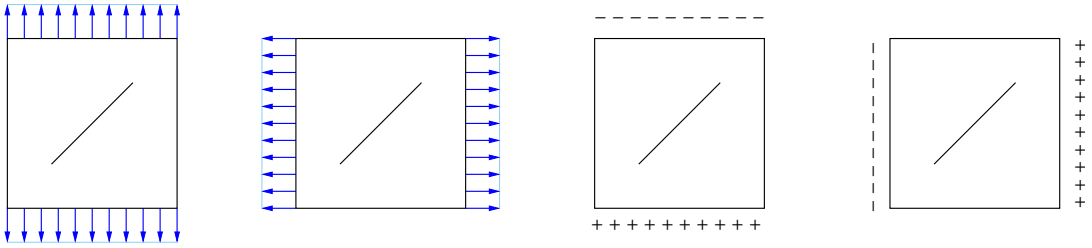

Figure 3: Illustration of the loads $F_m^{(1\mathrm{m})}$, $F_m^{(2\mathrm{m})}$, $g_m^{(1\mathrm{e})}$ and $g_m^{(2\mathrm{e})}$ in example 2

In example 2 with skew crack we choose the vertical and horizontal loads 1m and 2m. Additionally, we consider the purely electric load cases 1e and 2e, that also cause a vertical or horizontal crack opening, respectively, see Fig. 3.
Note that due to the material anisotropy, different states are generated by vertical and horizontal loads, respectively.
To provide simulated boundary data in place of real measurements, we use a forward computation with the variant SPC-PM2AdPiez of the 2D-FEM software package SPC-PM2Ad [9], written on the Chemnitz University of Technology. The inverse computation was implemented as postprocessing in this software.
Different levels of accuracy of these FEM generated synthetic data provide us with the possibility of assessing the effect of noisy data (in practice due to measurement errors) on the quality of our reconstructions.

5.2 FE-meshes and refinement strategies in the forward computation

In each example we start with a coarse mesh of 16 uniform squares (8×2 and 4×4 respectively), where each square is divided once into two triangular elements.
The simplest strategy to compute a preciser solution is uniform mesh refinement, where the next refinement level results from splitting each element into four sub elements (red division). In example 2, three additional refinement strategies have been tested for comparison. Besides the red division, also a green division (splitting of an element into two sub elements) was allowed to guarantee conforming meshes without hanging nodes.

- **adaptive refinement**
  This strategy applies a residual based error estimator, that means we examine the approximate FEM-solution u, φ on the current mesh refinement level to obtain information where the mesh should be refined [16]. Especially edge jumps of $\sigma(u,\varphi)n$ and $D(u,\varphi)n$ are considered in order to detect edges to be marked for refinement [7],[13].

- **(exclusive) boundary concentrated refinement**
  In each step, only all edges on the outer boundary are marked for refinement. This leads to refinement of all elements on the boundary, with a red-green closure to the inner domain Some details on the boundary concentrated FEM can be found for e.g., in [3], [6].

- **combined adaptive and boundary concentrated refinement**
  In this combined strategy, all boundary edges are marked for refinement in addition to those marked by the error estimator, in order to achieve a good solution in the whole domain with especially fine resolution on the boundary.

All these strategies follow the intention to obtain an approximate solution, which has a good accuracy, but needs a significantly lower number of nodes and elements than the one obtained from a uniform refinement. The idea of using boundary concentrated strategies is motivated by the fact, that the inverse computation evaluates only boundary integrals.
To illustrate all refinement strategies used here, the deformed meshes in each case are illustrated after refinement up to more than 4000 nodes in Fig. 4.

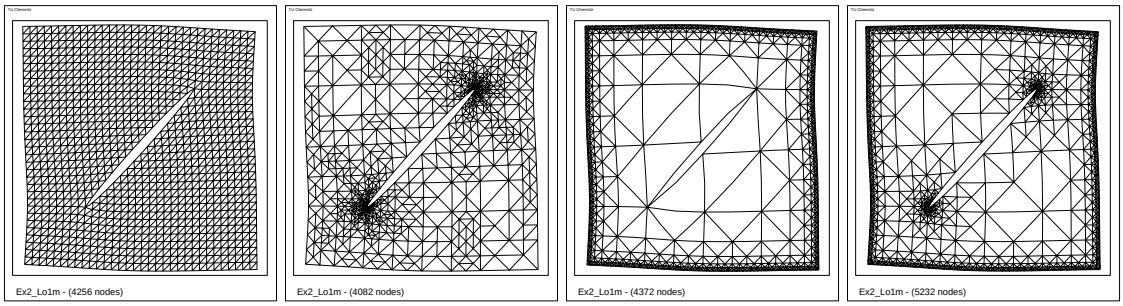

Figure 4: Deformed meshes obtained by uniform, adaptive, boundary concentrated and a combined adaptive and boundary concentrated mesh refinement

Computation of the boundary integrals

The computation of $RG(v,\psi)$ (13),(14) requires the integration of

$$v^\top F_m \ , \quad \mathfrak{n}^\top \sigma(v,\psi) u_m \ , \quad \psi g_m \quad \text{and} \quad \mathfrak{n}^\top D(v,\psi)\varphi_m$$

along each boundary edge E. We use a quadratic approximation of u and φ as well as linearly approximated F_m and g_m in each element. Since v, ψ are of polynomial degree less than or equal to two, each summand of the integrand has a maximal polynomial degree of three, so that SIMPSON's rule provides an exact integration of $RG(v,\psi)$ regarding the approximate solution along the edge.

5.3 Results with uniform refinement

5.3.1 Determination of the crack normal

Determination of the crack normal is carried out as described in section 2 according to variants a) and b). In example 1 both variants yield reasonable results for the angle, as comparison with the correct solution $\phi = 0$ show, see Fig. 5, where we plot the development for increasing refinement in the FEM simulation of the data. Also the error in the reconstructed angle is displayed in comparison with the purely elastic case. Here we plot the absolute values of the reconstructed angles versus the number of nodes in the first load case on a logarithmic scale along both axes. It can be seen that convergence in case of piezoelectric material as compared to the purely elastic case is not significantly slower.
In example 2 investigations are somewhat more extended, here four load cases have to be evaluated. In Fig. 6 the computational results of both variants are displayed and compared with the correct angle $\phi^* = -\frac{\pi}{4}$. Here it turns out that the loads 1e and 2e yields almost the same angle with each variant.
When using variant a) with the load case 2m a drastic error is observed at a coarser discretization,

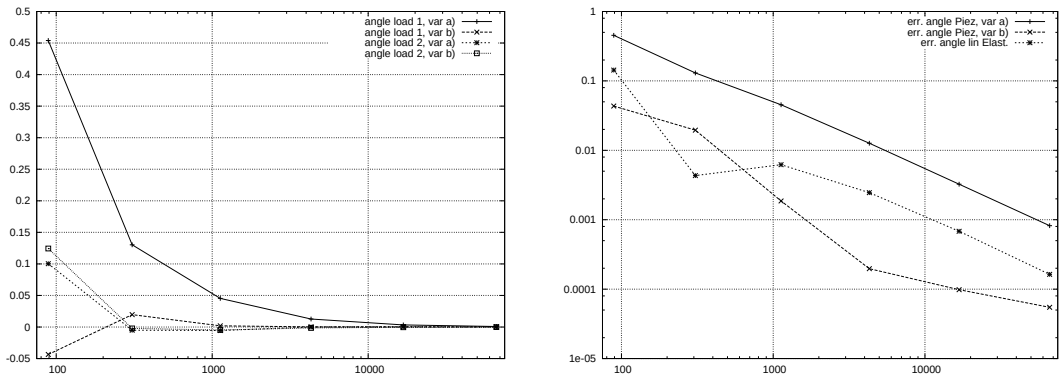

Figure 5: Reconstruction of crack angle (left) and errors in comparison to purely elastic material (right) for increasing number of nodes in FEM simulation of boundary data, example 1

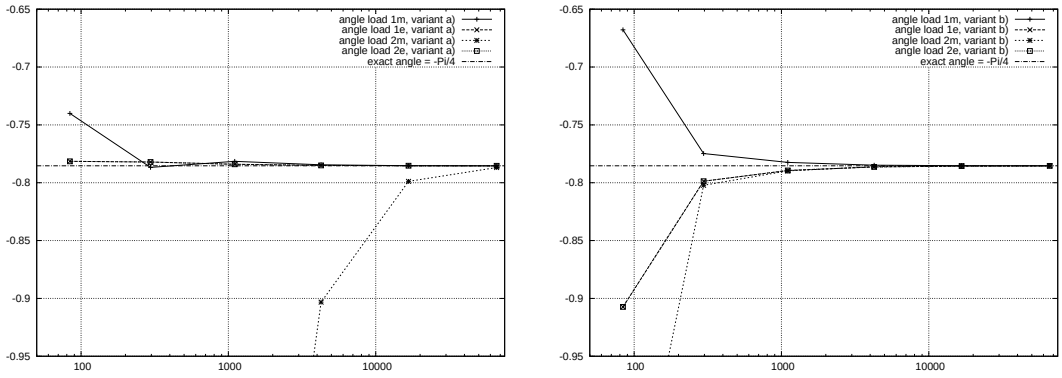

Figure 6: Reconstruction of crack angle with variants a) (left) and b) (right) of Subsection 2.1 in example 2

only after multiple refinement the computed angle approximates the exact one. The reason for this behaviour is the relatively small resulting potential jump over the crack,(see Fig. 7) which results in a reduced sensitivity of the inverse method. The large initial deviation in load case 2m

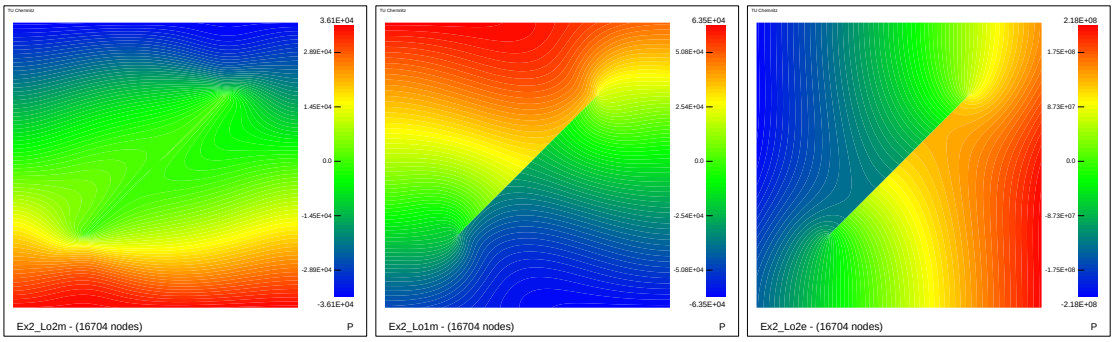

Figure 7: Potentials in load case 2m (left) in comparison to load cases 1m and 2e in example 2

of variant b) results from the fact that due to numerical errors an infeasible matrix R is generated. The diagonal shift modification of R described in Section 2.3 enables the computation of the admissible angle $\phi \approx -1.14$, but just leaves some error in the result. After the first refinement step, the errors are in the order of magnitude of the other load cases.

To investigate convergence of the computed angles to the exact one $\phi^* = -\frac{\pi}{4}$ with proceeding refinement we consider the abolute values of the deviations from ϕ^*. In Fig. 8 these are shown in double logarithmic scale with respect to the number of nodes in all four load cases, with variant a) and b). Here we compare the errors both under the horizontal loads 2m, 2e and under the

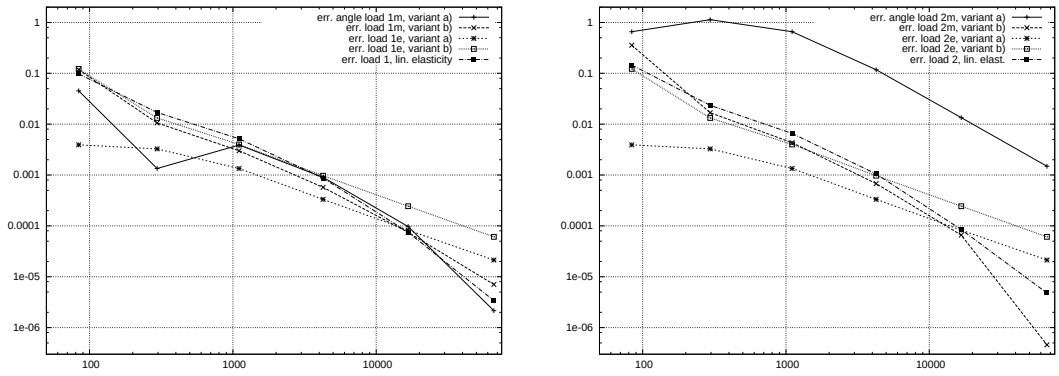

Figure 8: Errors in crack angle with variants a) and b) of Subsection 2.1 in example 2 for piezoelectric material in comparison with the purelay elastic case (with a reconstruction method corresponding to variant b)) under horizontal (left) and vertical (right) loads.

vertical ones 1m, 1e, with the results for purely elastic materials, where approximately the same convergence behaviour can be observed.

5.3.2 Determination of the crack plane distance to the origin and the approximate mid point coordinate

Assuming the crack normal to be known, determination of the constant according to Section 3 was carried out with both variants a) and b).

Here we use the additional terms with the parameters γ_E and γ_T (cf. Section 3.3). The use of $\gamma_{E,\sigma}$- and $\gamma_{T,\sigma}$-terms shows a tendency to less numerical stability in numerical tests. Moreover, for the special case $\phi = 0$ no admissible $\gamma_{T,\sigma}$ exists, while $\gamma_{E,\sigma}$ can be chosen arbitrarily but is not automatically set to zero as is the case for γ_E.
In example 1 this leads to a good convergence to the exact solution $C^* = 1$ in both variants.
In example 2, computations were carried out for all load cases, the results for each of the two variants a) and b) are shown in Fig. 9. Here again difficulties arise as expected in variant a) in

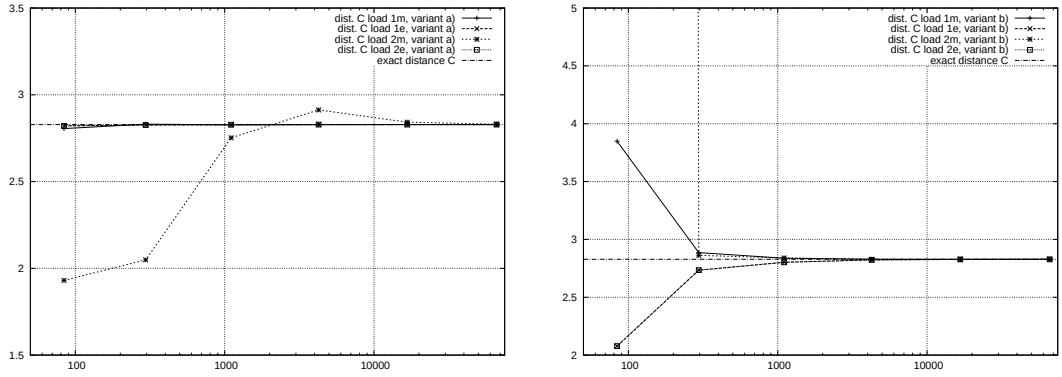

Figure 9: Reconstructed crack constant C with variants a) (left) and b) (right) in example 2

load case 2m, where due to the small potential jump convergence to the exact constant $C = 2\sqrt{2}$ only takes effect for sufficienly fine meshes.
In variant b) with load case 2m we only observe an outlier in the 0th refinement step, due to an infeasible matrix R which leads to a division by zero in (28) after stabilization. After the first refinement step, computations yield good results for all load cases.

To compare the speed of convergence among the different variants and with the purely elastic case, we look on the deviation of the numerically determined crack plane constants from the exact values $C^* = 1$ in example 1 and $C^* = 2\sqrt{2}$ in example 2.
Figure 10 shows the deviations depending on the number of nodes, P1 and P2 denoting the examples with piezo material and LE1,LE2 denoting the corresponding linear elastic examples.

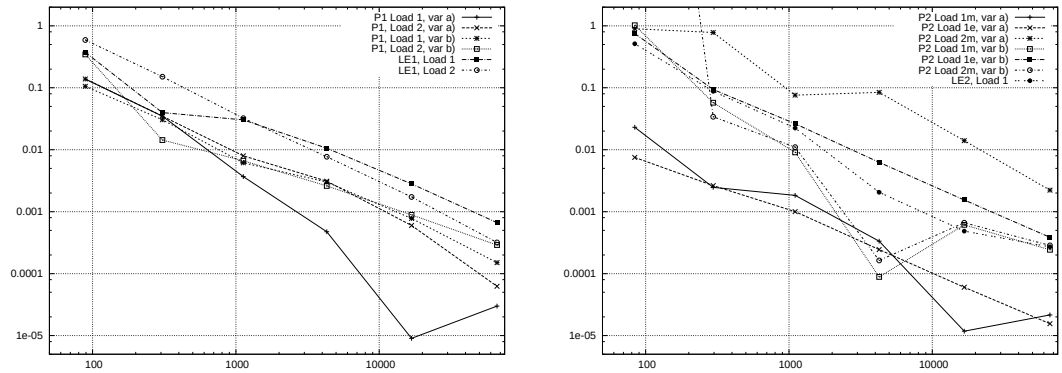

Figure 10: Comparison of errors in reconstructed plane constant C for piezoelectric and for purely elastic material in example 1 (left) and 2 (right).

There is basically no difference in the convergence speed. In example 2 the convergence rate of variant a) is the same as in b) and linear elasticity, convergence just takes effect with a bit of delay

in the load case 2m but starts from a slightly lower level in the other load cases.
Furthermore, a mid point approximation using variants a) and b) from Section 4 was computed in the second crack example (with single crack). Figure 11 shows that the convergence behaviour is comparable to the one for the crack plane parameters.

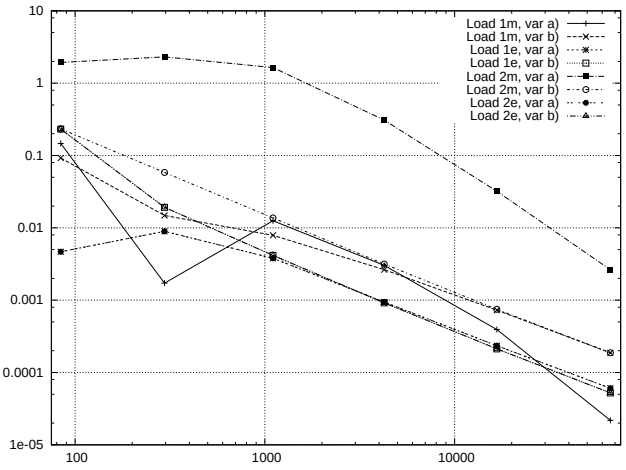

Figure 11: Deviations of the approximated mid point coordinate from the true value in example 2

5.4 Comparison of results with different refinement strategies

For example 2 all four refinement strategies were investigated with respect to their results in the inverse computations. The development of the deviations of the crack plane angle and the distance to the origin from the respective exact values are shown in Figure 12 for the load case 1m.
When using boundary concentrated refinement with or without additional interior adaptivity, the errors are significantly lower with the same number of nodes in sufficient fine meshes. Especially in variant b) the difference is obvious from the figures. The worst results are observed in the case of usual adaptively refined meshes, where the outer boundary is refined only sparsely. We conjecture that the reason for this effect is a concentration of the adaptive refinement to the surroundings of the crack tips, where stress singularities occur. However, if the crack tips are sufficiently far away from the outer boundary, no pollution effect seems to be visible to the boundary integral, so that this refinement at the crack tips leads to unnecessary additional degrees of freedom.

Acknowledgement

We gratefully acknowledge the German research foundation (DFG) for financial support of the project "Risse in Piezokeramiken" under grant numbers KA 1778/1 and SA 539/4-1. Thanks go also to the TU Chemnitz for providing the FEM software SPC-PM 2Ad and A.-M. Sändig for useful suggestions and discussion.

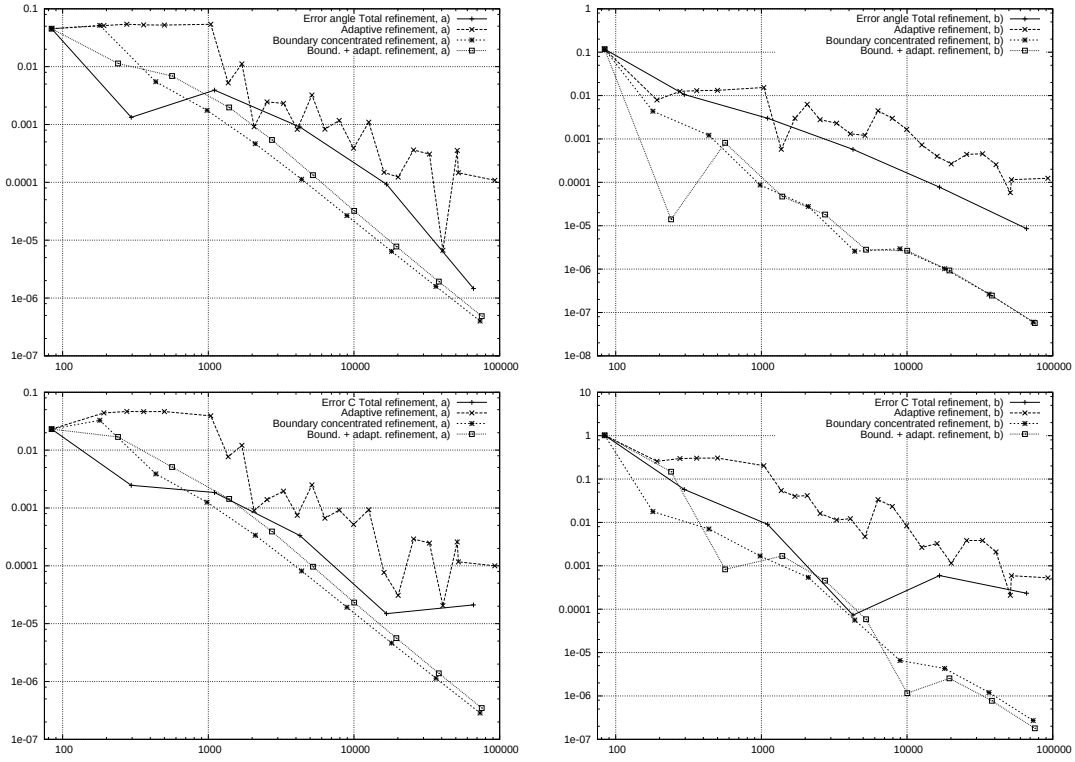

Figure 12: Comparison of the crack plane angle (upper) and offset (lower) deviation in variant a) (left) and b) (right) for the load case 1m in example 2

References

[1] S. Andrieux, A. Ben Abda and H. D. Bui: *Reciprocity principle and crack identification.* Inverse Problems 15, 1999, 59-65

[2] S. Andrieux and A. Ben Abda: *Identification of planar cracks by complete overdetermined data: inversion formulae.* Inverse Problems 12, 1996, 553-563

[3] T. Eibner: *Randkonzentrierte und adaptive hp-FEM.* Dissertation, TU Chemnitz, 2006

[4] T. H. Hao and Z. Y. Shen: *A new electric boundary condition of electric fracture mechanics and its applications.* Engineering Fracture Mechanics 47, 1994 p. 793-802

[5] G. Kemmer and H. Balke: *Krafteinwirkungen auf die Flanken nichtleitender Risse in Piezoelektrika.* In: GAMM 98, Short Communications in Mathematics and Mechanics, ZAMM Vol. 79 S2, 1999, p. 509-510

[6] B. I. Khoromskij and J. M. Melenk: *Boundary concentrated FEM* SIAM J. Numer. Anal., 41:1-36, 2003.

[7] G. Kunert and R. Verfürth: *Edge Residuals dominate a posteriori Error Estimates for Linear Finite Element Methods on anisotropic triangular and tetrahedral meshes.* Numer. Math., 86:283-303, 2000.

[8] A. Lenk: *Elektromechanische Systeme, Band 2 (Systeme mit verteilten Parametern).* VEB Verlag Technik, Berlin, 1974

[9] A. Meyer: *Programmer's Manual for Adaptive Finite Element Code SPC-PM 2Ad.* Preprintenreihe des SFB 393, Preprint 01-18, TU Chemnitz, 2001

[10] A. Meyer and P. Steinhorst: *Modellierung und Numerik wachsender Risse bei piezoelektrischem Material.* Preprint CSC/10-01, TU Chemnitz, 2010

[11] S. B. Park and C. T. Sun: *Effect of electric field on fracture of piezoelectric ceramics.* International Journal of Fracture, 1995, 70:203-216

[12] M. Scherzer and M. Kuna: *Combined analytical and numerical solution of 2D interface corner configurations between dissimilar piezoelectric materials.* International Journal of Fracture, 2004, 127:61-99

[13] P. Steinhorst: *Anwendung adaptiver FEM für piezoelektrische und spezielle mechanische Probleme.* Dissertation, TU Chemnitz, 2009

[14] P. Steinhorst and A. M. Sändig: *Reciprocity principle for the detection of planar cracks in anisotropic elastic material.* Preprint IANS-2010/011, Universität Stuttgart, 2010

[15] A. Valean: *Identifikation von planaren Rissen in der Piezoelektrizität.* Diplomarbeit, Universität Stuttgart, 2010

[16] R. Verfürth: *A review of a posteriori error estimation and adaptive mesh-refinement techniques.* Wiley-Teubner series advances in numerical mathematics, Chichester, Stuttgart, 1996.